Altered growth characteristics of skin fibroblasts from wild-derived mice, and genetic loci regulating fibroblast clone size

Rong Yuan,[1] Kevin Flurkey,[1] Renee Van Aelst-Bouma,[1] Weidong Zhang,[1] Benjamin King,[1] Steve Austad,[2] Richard A. Miller[3] and David E. Harrison[1]

[1]The Jackson Laboratory, 600 Main Street, Bar Harbor, ME 04609, USA
[2]Department of Cellular & Structural Biology, Barshop Institute for Longevity & Aging Studies, University of Texas Health Science Center, 15355 Lambda Drive, STCBM Bldg. 3.100, San Antonio, TX 78245, USA
[3]Department of Pathology, Geriatrics Center, and VA GRECC, University of Michigan School of Medicine, 5316 CCGCB, Box 0940, 1500 E. Medical Center Drive, Ann Arbor, MI 48109, USA

Summary

Mouse fibroblast senescence *in vitro* is an important model for the study of aging at cellular level. However, common laboratory mouse strains may have lost some important allele variations related to aging processes. In this study, growth *in vitro* of tail skin fibroblasts (TSFs) derived from a wild-derived stock, Pohnpei (Pohn) mice, differed from growth of control C57BL/6 J (B6) TSFs. Pohn TSFs exhibited higher proliferative ability, fewer apoptotic cells, decreased expression of *Cip1*, smaller surface areas, fewer cells positive for senescence associated-β-galactosidase (SA-β-gal) and greater resistance to H_2O_2-induced SA-β-gal staining and *Cip1* expression. These data suggest that TSFs from Pohn mice resist cellular senescence-like changes. Using large clone ratio (LCR) as the phenotype, a quantitative trait locus (QTL) analysis in a Pohn/B6 backcross population found four QTLs for LCR: *Fcs1* on Chr 3 at 55 cM; *Fcs2* on Chr X at 50 cM; *Fcs3* on Chr 4 at 51 cM and *Fcs4* on Chr 10 at 25 cM. Together, these four QTLs explain 26.1% of the variations in LCRs in the N2 population. These are the first QTLs reported that regulate fibroblast growth. Glutathione S transferase mu (*GST-mu*) genes are overrepresented in the 95% confidence interval of *Fcs1*, and Pohn TSFs have higher H_2O_2-induced *GST-mu 4*, *5* and *7* mRNA levels than B6 TSFs. These enzymes may protect Pohn TSFs from oxidation.
Key words: fibroblast; oxidative stress (OS); quantitative trait locus (QTL).

Correspondence

David E. Harrison, The Jackson Laboratory, 600 Main Street, Bar Harbor, Maine 04609, USA. Tel.: 207-288-6357; fax: 207-288-6687; e-mail: david.harrison@jax.org

Introduction

When fibroblasts are isolated and cultured, they initially divide rapidly. But after a characteristic number of cell divisions, their ability to proliferate is gradually reduced. After this period of slower growth, human fibroblasts enter a state of growth arrest termed replicative senescence (RS) (Hayflick, 1965). Mouse fibroblasts, however, enter a second period of accelerated growth that represents the emergence of an immortalized cell line (Hornsby, 2003; Cristofalo *et al.*, 2004; Itahana *et al.*, 2004).

Human fibroblasts enter RS mostly because of the shortening of telomeres and the low activity of telomerase (Masutomi *et al.*, 2003). In contrast, because of their extremely long telomeres, mouse fibroblasts avoid this and instead oxidative stress (OS) may play a critical role in growth arrest of mouse fibroblasts (Hornsby, 2003; Parrinello *et al.*, 2003; Itahana *et al.*, 2004). Human cell RS is also affected by oxidative stress, since over-expression of superoxide dismutase, an antioxidative stress gene in human fibroblasts, decreases the intracellular peroxide content, retards the telomere shortening rate, and prolongs the lifespan of these cells under normoxia and hyperoxia (Serra *et al.*, 2000, 2003). Thus, studies on regulation of mouse fibroblast growth may also be relevant to mechanisms of RS in human cells.

The mice used in this study are from a wild-derived mouse stock Pohnpei (Pohn), descended from four founders trapped on the South Pacific island of Pohnpei. Because of the constant climate and low murine predation on the island, evolutionary theory predicts that slower aging rates might have evolved (Williams, 1957; Charlesworth, 1980; Austad, 1996; Miller *et al.*, 2000a). Furthermore, wild-derived strains may provide genetic variation missing from standard laboratory inbred strains (Klebanov *et al.*, 2001a,b). Although mean lifespan is not abnormally long in an independent stock descended from progenitors trapped at the same time and place (Miller, 2000b), when compared to standard inbred strains, Pohn mice show characteristics that may relate to retarded aging: smaller body size, slower body growth, and longer female reproductive lifespans (unpublished observations).

The current study shows that Pohn TSFs have very high large clone ratios (LCRs) at young and old ages, and resist apoptosis and oxidative stress. We identify four loci in Pohn mice that regulate LCRs. Previous studies have identified quantitative trait loci (QTLs) that regulate age-related phenotypes such as lifespan (Geiger-Thornsberry & Mackay, 2004), growth (Vaughn *et al.*, 1999), and T-cell subsets (Jackson *et al.*, 2003). But, although *in vitro* fibroblast RS has been used as a cellular model for aging studies for about 40 years, and although many genes have been reported to affect RS, no QTLs have been reported that regulate fibroblast growth. These results are a step in defining genetic regulation of growth and senescence in mammalian cells.
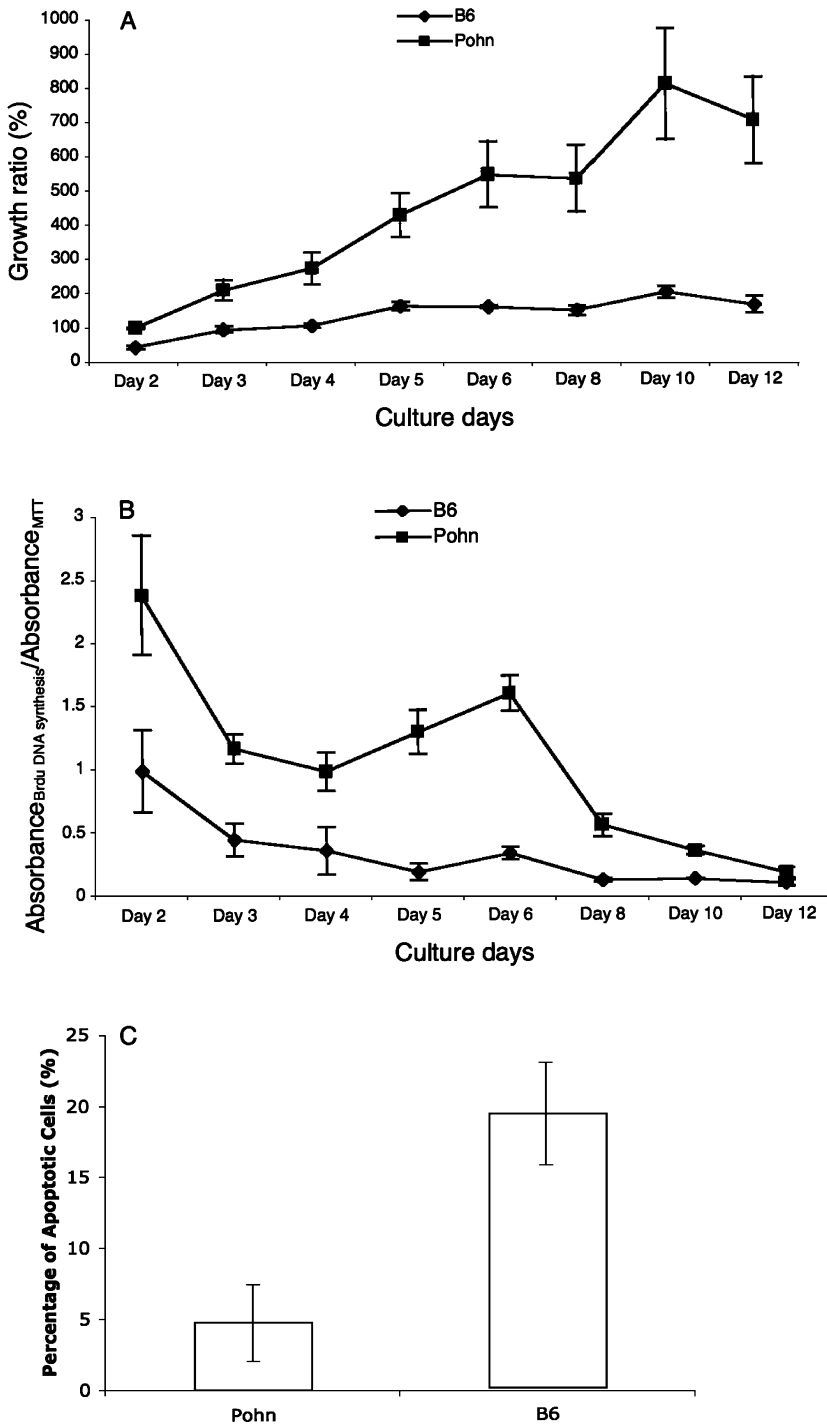
Fig. 1 (A) Pohn and B6 tail skin fibroblast (TSF) growth rates were measured using MTT. Pohn fibroblasts have significantly higher growth rates at all time points from 2 to 12 days ($P < 0.05$, $n = 6$; n values are for each strain at each point throughout; error bars show SEM). (B) DNA synthesis, measured by uptake of BrdU, decreases with culture time in both strains. DNA synthesis rates are significantly higher in Pohn TSFs than in B6 TSFs, at all time points, from 2 to 12 days. DNA synthesis was normalized for cell number using MTT absorbance as a measure of cell number. ($P < 0.05$, $n = 6$; error bars show SEM). (C) On day 7 of cell culture, the percentage of apoptotic B6 TSFs is significantly greater than that of Pohn TSFs ($19.3.0\% \pm 3.6\%$ and $4.7\% \pm 2.7\%$, respectively; $P < 0.05$, $n = 3$; error bars show SD).

Results

Increased proliferation and decreased apoptosis of Pohn TSFs

Pohn TSF growth ratios measured by the MTT [3-(4, 5-dimethyl-thiazolyl-2)-2, 5-diphenyltetrazolium bromide] cell proliferation assay for viability were significantly higher than those for B6 at all time points from day 2 on (Fig. 1A). This was confirmed using BrdU uptake to measure the rate of DNA synthesis. In Pohn mice, the TSF DNA synthesis rates were significantly higher than those of B6 TSFs at all time points (Fig. 1B). Annexin V-PE and propidium iodide (Ling *et al.*, 2002) dual-labeling methods revealed that after 7 days of culture, numbers of apoptotic B6 TSFs were about four times greater than those of Pohn TSFs (Fig. 1C).
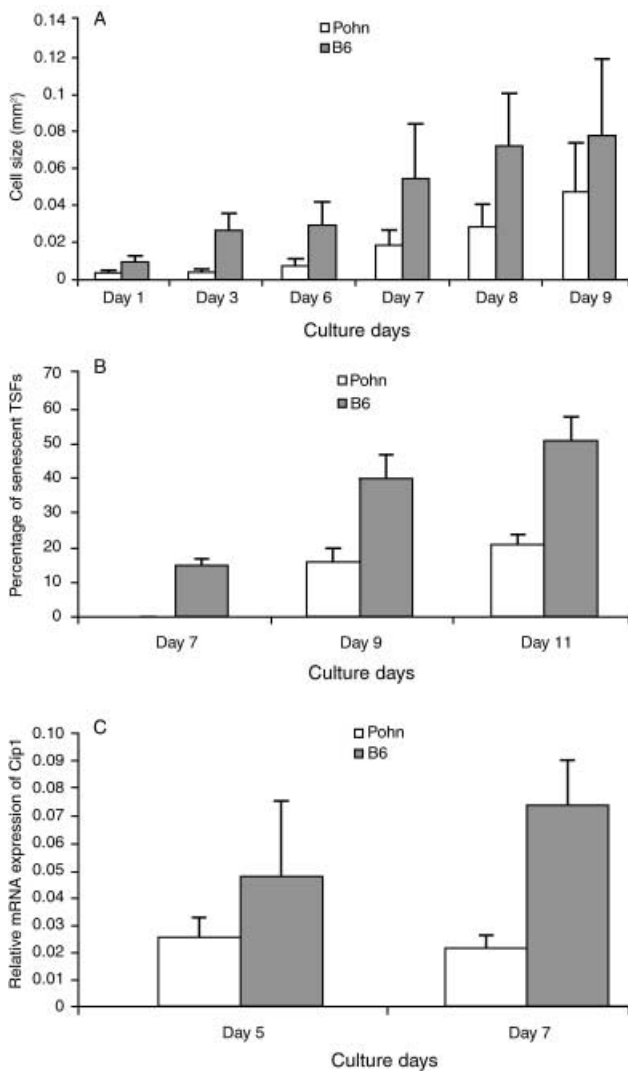
Fig. 2 (A) The cell surface areas of Pohn and B6 TSFs were measured at 1, 3, 6, 7, 8 and 9 days after cells were seeded. For both strains, cell size increases with time. However, at all time points, except day 9, B6 TSF sizes are significantly larger than those of Pohn TSFs ($P < 0.05$, $n = 6$; error bars show SEM). (B) SA-β-gal staining in Pohn and B6 TSFs. SA-β-gal positive B6 TSFs were found from day 7, and numbers increased with time. No SA-β-gal positive Pohn TSFs were found until day 9; then numbers also increased with time. At all three time points, TSFs of B6 mice have significantly more SA-β-gal positive cells than those of Pohn mice ($P < 0.05$, $n = 6$; error bars show SEM). (C) *Cip1* mRNA expression in Pohn and B6 TSFs. At days 5 and 7, *Cip1* expression levels in Pohn and B6 TSFs were measured by real-time RT-PCR. At both time points, B6 TSFs have higher expression levels of *Cip1* than Pohn TSFs, and at day 7, this difference is significant ($P < 0.05$, $n = 3$–8; error bars show SEM).

Resistance to TSF senescence-like changes in Pohn mice

Senescent cells exhibit a larger surface area than actively growing cells (Kumazaki *et al.*, 1991; Berube *et al.*, 1998). Cell surface areas increased with culture time for both Pohn and B6 cells, but at all time points, B6 TSFs were much larger than Pohn TSFs (Fig. 2A).

β-Galactosidase (β-gal) activity is scattered in young cells, but clustered in senescent cells, suggesting a predominance of autolysosomes (Gerland *et al.*, 2003), and making β-gal positive a marker for aging cells *in vitro* and *in vivo* (Krishnamurthy *et al.*, 2004). We tested senescence associate-β-gal (SA-β-gal) in TSFs derived from six Pohn and six B6 mice on days 3, 5, 7, 9 and 11 after cells were seeded. SA-β-gal stained B6 TSFs were present on day 7. SA-β-gal stained Pohn TSFs did not appear until day 9, and the percentage was significantly lower than in B6 TSFs (Fig. 2B).

CIP1 is a potent cyclin-dependent kinase inhibitor and is involved in cell cycle arrest, differentiation and apoptosis as a downstream mediator of p53. Previous studies in human and mouse cells suggest that increased expression of *Cip1* is a molecular marker for cell senescence (el-Deiry *et al.*, 1993; Brown *et al.*, 1997; Chen *et al.*, 2002; de Haan *et al.*, 2004). Real-time RT-PCR showed that between days 5 and 7 after cells were seeded, the *Cip1* mRNA level increased in B6 TSFs, while it decreased slightly in Pohn TSFs. At both time points, B6 TSFs expressed more *Cip1* than Pohn TSFs; this difference was significant at day 7 (Fig. 2C).

Pohn fibroblast resistance to H₂O₂

Oxidative stress appears to accelerate senescence both *in vivo* and *in vitro*. We treated TSFs with H_2O_2 for 2 h. After 24 h, we found SA-β-gal positive cells in B6 TSFs treated with an H_2O_2 concentration as low as 10 μM; SA-β-gal positive cell numbers increased as the H_2O_2 concentration increased. In Pohn TSFs, SA-β-gal positive cells were found only in the group treated with 640 μM H_2O_2 (Fig. 3A).

Using 160 μM H_2O_2 to induce *Cip1* expression assayed by real-time RT-PCR, in B6 TSFs, 4, 8 and 24 h after the treatment, *Cip1* mRNA levels were significantly higher than normal levels, 6.3-, 4.2-, and 6-fold, respectively. However, in Pohn TSFs, 160 μM H_2O_2 induced less than 2-fold increases in *Cip1* expression after 4 and 8 h, and *Cip1* mRNA levels decreased to the level of untreated cells by 24 h (Fig. 3B).

Higher LCR of Pohn TSFs throughout life

TSFs from Pohn mice show much higher LCR 7 days after plating than those from the long-lived standard B6 strain. LCRs significantly decrease in old mice of both groups, but, whether young or old, Pohn mouse TSFs have LCRs about fourfold higher than TSFs from B6 mice. LCRs for young Pohn mice are also significantly higher than those in (Pohn $\times$ B6) F_1 hybrid mice (Table 1). Thus, the Pohn alleles for high LCRs are recessive in Pohn $\times$ B6 F_1 mice. Because the ratio of Pohn to B6 LCRs is 3.7 when both are young, and 4.4 when both are old, the advantage of Pohn cells is not exhausted over the lifespan (Table 1).

QTL analysis for high LCRs in Pohn mice

To find the loci that regulate for LCRs, we produced 162 N2 mice by backcrossing Pohn $\times$ B6 F_1 females with Pohn males.
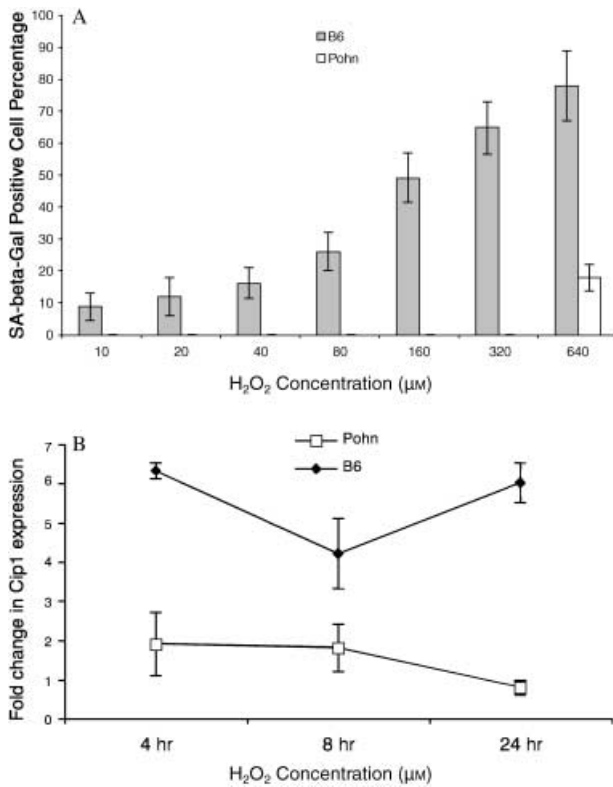
Fig. 3 (A) B6 and Pohn TSFs were treated with H_2O_2 for 2 h. After 24 h, senescent cells were counted by SA-β-gal staining. SA-β-gal positive cells are found in B6 TSFs treated with H_2O_2 concentrations as low as 10 μM. In Pohn mouse TSFs, senescent cells are found only in the group treated with 640 μM H_2O_2. (n = 3; data are given as mean ± SEM). (B) *Cip1* expression induced by 160 μM H_2O_2 in Pohn and B6 TSFs. At all time points, the fold changes of *Cip1* mRNA levels in B6 are significantly greater than in Pohn (P < 0.05, n = 3; data shown as mean ± SEM).

Table 1 Large clone ratios (LCRs) of Pohn, B6 and Pohn × B6 F_1 tail skin fibroblasts (TSFs)

	Young	Old
Pohn	60.2 ± 8.9*,**,***	28.4 ± 5.6
B6	16.2 ± 3.4***	6.4 ± 2.5
Pohn × B6 F_1	21.2 ± 5.2	NA

TSF LCRs were measured in young (6- to 10-week-old) and old (18- to 24-month-old) mice. *Compared to B6, $P < 0.05$; **compared to Pohn × B6 F_1, $P < 0.05$; ***compared to old age, $P < 0.05$. Data is shown as mean + SEM (n = 6–15).

Epistatic effects (gene–gene interactions) estimated by pairwise scanning identified strong interactions for QTLs on Chr 4 (51 CM) and Chr 10 (25 CM). Both have low LOD scores in the single QTL scan (LOD < 1.5), however, the LOD score of the interaction between these QTLs is 3.8, and the joint LOD score is 4.7, both highly significant (Tables 2 and Fig. S2). These interactive QTLs were named *Fcs3* (Chr 4) and *Fcs4* (Chr 10).

Table 2 shows multiple regression results, taking into account effects of gender, *Fcs1*, *Fcs2*, *Fcs3*, *Fcs4* and significant interactions. The whole model explains 26.1% of the total variance for the LCR. *Fcs1* alone explains 5.3% of the total variance. *Fcs2* and the interaction of *Fcs2* with gender explain 5.1% of the total variance, while the interaction alone explains 4.9% of the variance. Thus, the main contribution of *Fcs2* to the LCR variation comes from the interaction with gender. *Fcs3* explains 9.0% of the total variance; *Fcs4* explains 8.9%. The interaction between the two QTLs accounts for nearly all of this (8.4%).

In the N2 population, mice with the homozygous Pohn *Fcs1* allele (P/P) had LCRs significantly higher than heterozygous mice (P/B), while in the interaction between *Fcs2* and gender, LCRs were similar in P/Y and B/Y males, but significantly lower in P/P than in heterozygous P/B females (Fig. 4). *Fcs3* and *Fcs4* have complex interactive effects, where heterozygosity (P/B) in either, with the homozygosity (P/P) of the other, is associated with increased LCRs; the lowest LCRs are found when both QTLs are homozygous (Fig. 4).

We tested 131 SNPs in each mouse (Table S1), and found suggestive QTLs for the LCR on Chr 3 [logarithm of odds (LOD) = 2.9 at 55 CM] and Chr X (LOD = 2.6 at 50 CM). These fibroblast clone size (FCS) QTLs were named *Fcs1* (Chr 3) and *Fcs2* (Chr X) (Table 2 and Fig. S1).

Table 2 Multiple regression model for loci affecting fibroblast large clone ratio

	QTL	Chr (cM)	d.f.	Type III SS	% variance	*F*-value	*P*-value
Gender*	/	/	2	984.8	6.1	5.1	0.007
Chr 3@55.01	*Fcs1*	Chr 3 (55)	1	859.2	5.3	8.9	0.003
Chr X@50	*Fcs2*	Chr X (50)	2	825.9	5.1*	4.3	0.016
Chr 4@51	*Fcs3*	Chr 4 (51)	2	1459.7	9.0*	7.6	0.001
Chr 10@25	*Fcs4*	Chr 10 (25)	2	1445.1	8.9*	7.5	0.001
Chr 4@51 x† Chr 10@25	/	/	1	1367.5	8.4	14.2	0.0002
ChrX@50 x† Gender	/	/	1	795.7	4.9	8.3	0.005

The P value for each term in the model is based on the F distribution with corresponding degrees of freedom. F-statistics from the multiple regression model are based on sums of squares (SS).
*Variances explained by a single component include their interaction effects.
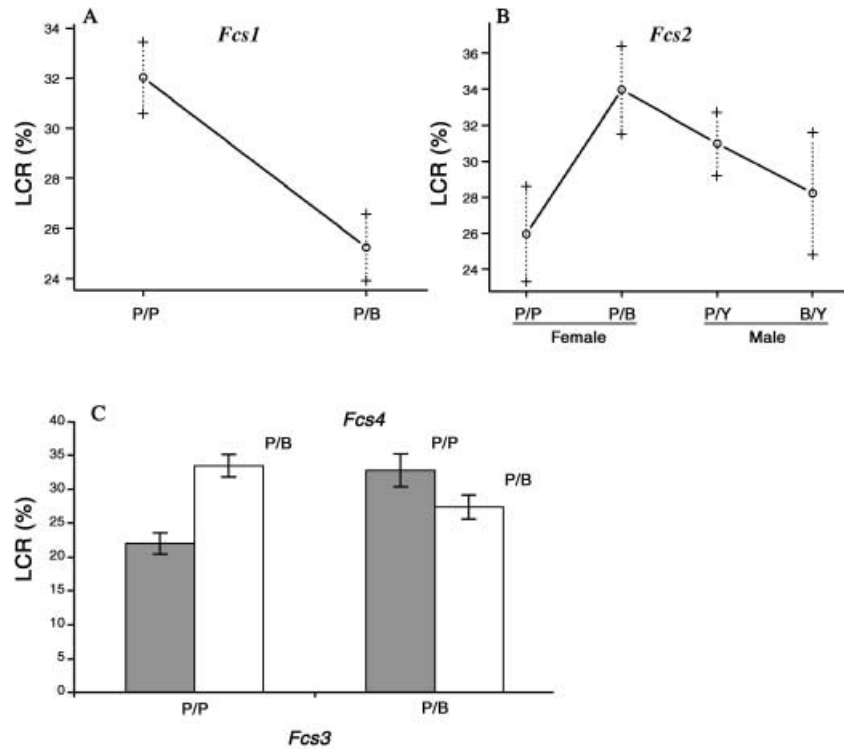†Lower-case x indicates gene–gene interaction.

Fig. 4 QTL and QTL interaction effects on LCRs in the N2 population. (A) For *Fcs1*, mice homozygous for Pohn alleles (P/P) had significantly higher LCRs than mice with heterozygous alleles (P/B) ($P < 0.05$). (B) For *Fcs2*, male mice with a Pohn allele (P/Y) had slightly higher LCRs than mice with a B6 allele (B/Y); however, female mice homozygous for Pohn alleles (P/P) had significantly lower LCRs than heterozygous mice (P/B) ($P < 0.05$). (C) For the interaction between *Fcs3* and *Fcs4*, heterozygosity of either of these two QTLs with the homozygous Pohn allele at the other had the highest LCRs, significantly higher than LCRs in mice with homozygous alleles at both QTLs ($P < 0.05$). Data shown as mean ± SEM ($n = 35–71$).
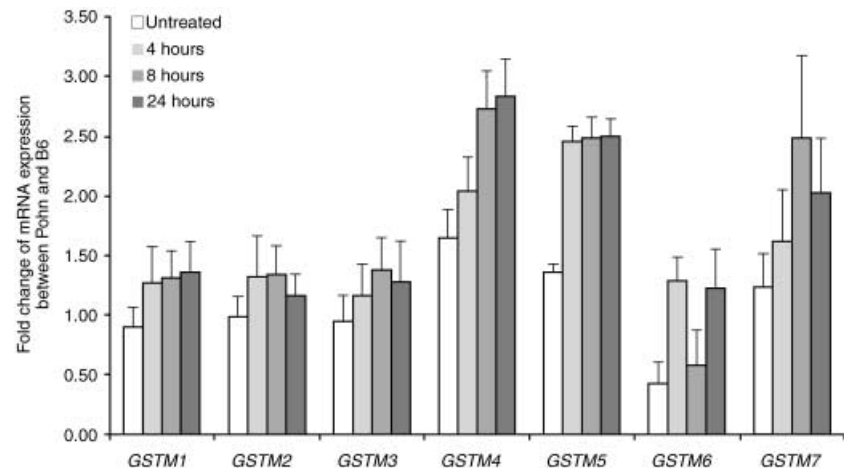

Fig. 5 Expression of *Gstm* genes in H_2O_2-treated Pohn and B6 TSFs. Pohn and B6 TSF cultures were treated with 160 μM H_2O_2 for 2 h. After 4, 8 and 24 h, the mRNA expression of *Gstm* genes was measured by real-time RT-PCR. The figure shows the fold change of mRNA expression between strains: Pohn TSFs/B6 TSFs; error bars show the SEM, $n = 6–9$.

Up-regulation in mRNA expression of Gstm genes in Pohn TSFs

Gene ontology analysis suggests that glutathione S-transferase (Gst) family mu class (Gstm) genes are over-represented in *Fcs1* (details are in S1 in the online supplementary experimental procedures and results). To test whether these genes may explain oxidation resistance, their expression was compared in Pohn and B6 TSFs before and after H_2O_2 treatment. Expression of *Gstm1*, *2* and *3* was similar in Pohn and B6 TSFs. *Gstm6* was down-regulated in untreated Pohn TSFs, but had similar expression levels in Pohn and B6 TSFs after H_2O_2 treatment. Expression of *Gstm5* and *7* was similar in untreated Pohn and B6 TSFs,

but increased in Pohn TSFs after H_2O_2 treatment 1.6- to 2.6-fold. *Gstm4* was more highly expressed in both untreated and H_2O_2-treated Pohn TSFs (Fig. 5).

Discussion

Reduced proliferative abilities might contribute to age-related physiological impairment and promote age-related disease in intact organisms, and may be modeled by decreased cell proliferation *in vitro*. Therefore, mice with high cell proliferation are of interest. Whether young or old donors are used, Pohn TSFs form much larger clones compared to B6 TSFs, proliferate more vigorously after initial plating, and subsequently lose

proliferative ability more slowly. Pohn fibroblasts also were superior in the following cell senescence markers: cell surface size, SA-β-gal positive cells and *Cip1* mRNA expression.

As the phenotype for QTL analysis, we used LCR (Smith *et al.*, 1978), as this assay integrates several features of cell growth *in vitro,* including cell proliferation and apoptosis. Importantly, LCR demonstrates the heterogeneity of cell populations, unlike cell population doublings, which are dominated by the proliferative potentials of the best clones (Angello & Prothero, 1989; Angello *et al.*, 1989; Pendergrass *et al.*, 1993). Clone size analysis is also less influenced by transformation events that produce frequent immortalization of mouse and rat cell populations (Stanulis-Praeger, 1987; Peacocke & Campisi, 1991; Pignolo *et al.*, 1992). Finally, the decrease in the age-related decline in LCRs by caloric restriction, the only nongenetic treatment that consistently extends mouse lifespan, supports the use of LCR as a biomarker of aging (Pendergrass *et al.*, 1995; Wolf *et al.*, 1995).

In this study, TSFs from the wild-derived Pohn stock have high LCRs and with young donors, 60% of the cells forming any clone (four or more cells) produce clones with more than 100 cells (Table 1). This is nearly fourfold higher than found in TSFs from the long-lived standard B6 inbred strain (16%), and threefold higher than found in TSFs from the F_1 hybrid of Pohn and B6 (21%). Other assays suggested that Pohn TSFs have high LCRs both because they proliferate faster and show less apoptosis. Although Pohn mice are only partially inbred, the similarity of B6 and the Pohn × B6 F_1 shows that the high LCRs in Pohn mice do not result from their hybrid vigor.

An increased susceptibility to apoptosis occurs in cells made senescent by exposure to OS (de Haan *et al.*, 2004). Mouse fibroblasts cultivated in 3% oxygen grow faster and reach higher saturation densities than those cultivated in 20% oxygen (Parrinello *et al.*, 2003). In a segmental progeroid mouse model, in which a proofreading-deficient version of the mitochondrial DNA polymerase γ (POLG) accumulates mtDNA mutations, there was no increase in markers of OS or accelerated mouse embryo fibroblast RS, although accelerated aging was observed in several organs and tissues (Kujoth *et al.*, 2005). These studies strongly suggest that mouse fibroblasts senesce as a result of OS. We found that after being cultivated for 7 days, there are about four times more apoptotic cells in B6 fibroblasts than in Pohn fibroblasts (Fig. 1C). Thus despite faster proliferation (and therefore more energy use) in Pohn compared with B6 TSFs, Pohn cells resist other senescence-like changes. The hypothesis that Pohn TSFs have increased resistance to OS is supported by resistance to H_2O_2. For B6 TSFs, SA-β-gal staining positive cells could be found in cells treated with as little as 10 μM H_2O_2, while Pohn TSFs were far more resistant, 640 μM was needed. The molecular senescence marker, *Cip1*, was far less induced in Pohn TSFs than in B6 TSFs (Fig. 3). Thus, in Pohn TSFs, greater ability to resist OS may play a role in retarding senescence-like changes and increasing LCR.

QTL analysis does not depend on preconceived ideas about how LCR is regulated, but rather provides entry points from which to investigate the regulating cellular and molecular pathways. In a backcross (N2) population between Pohn and B6, we identified four QTLs, including one interacting pair. Multiple regression showed that these QTLs explained a good part, 26.1%, of the variation in the whole population (Table 2). *Fcs1* alone explains 5.3% of the variation, and N2 mice with the Pohn homozygous allele in N2 population have significantly higher LCRs than mice with heterozygous B6/Pohn alleles (Fig. 4). *Fcs1* is colocalized with a previously detected QTL for regulating resistance to OS in the alloxan resistant (ALR) mouse strain (Mathews *et al.*, 2002).

In *Fcs1*, *Gstm* genes are overrepresented (online supplementary results). The *Gst* gene family is important for resistance to OS, because these genes catalyze the conjugation of compounds that can accumulate from OS and induce cell apoptosis (Ishikawa *et al.*, 1986; Spitz *et al.*, 1991; Cheng *et al.*, 2001). Expression of *Gst* family genes was elevated in the *daf-2* mutant nematode, which has increased adult lifespans (McElwee *et al.*, 2004). Our results exclude *Gstm1*, *2*, and *3* as candidates, because they have similar expression levels in Pohn and B6 cells, but *Gstm4*, *Gstm5* and *Gstm7* are up-regulated in H_2O_2-treated Pohn TSFs compared with B6 TSFs (Fig. 5), and may play a role in the enhanced OS resistance of Pohn TSFs.

Conclusion

When cultivated *in vitro*, TSFs from the wild-derived mouse stock, Pohn, resist senescence-like changes and OS compared with TSFs from B6 mice. By QTL analysis of LCRs, we discovered the first genetic loci that regulate fibroblast clone size in normal mammalian cell populations. As expected, LCR is a complex phenotype, with two single loci that have important effects, and two loci that have a very strong interaction. These results are consistent with the hypothesis that OS is related to cellular aging, and with the evolutionary theory that the alleles that facilitate slower aging rates might be found in wild populations in low hazard environmental niches.

Experimental procedures

Mice

Pohn mice were trapped on Pohnpei Island (7°N, 158°E) in the Federated States of Micronesia, at the same location and by the same methods as PoWC mice (Miller, 2000). The Pohn stock was generated from four mice (one female and three males) and is maintained at The Jackson Laboratory. F_1 hybrids were produced by crossing female Pohn mice with male B6 mice; a backcross population (N2) was produced by mating female F_1 mice with male Pohn mice. Thus, all N2 mice had Pohn mitochondria DNA. All mice received a pasteurized NIH-31 4% fat diet made by Purina and acidified water *ad libitum*. In the current study, 6- to 10-week-old mice were used throughout except for the 18- to 24-month-old mice used for tests of LCRs at old ages.

Isolation of TSFs

Following anesthesia, the whole tail was surgically removed and immersed in 50% ethanol for 20 min. The skin was stripped from the tail, washed with phosphate-buffered saline (PBS), cut into 2 mm pieces, and suspended and shaken gently in digestion solution (1% Dispase/Collagenase, Roche) at 37 °C for 3.5 h. The tissue was mixed with versene buffer (PBS containing 0.5 mM EDTA, Gibco Invitrogen Corp.) to inactivate proteases, and then washed twice with PBS. Cells were seeded in 25-cm^2 flasks using about 5×10^4/flask and cultivated in air with 5% CO_2 in culture medium containing Dulbecco's modified Eagle's medium (DMEM), 10% fetal bovine serum (FBS), 50 units mL^{-1} penicillin, and 50 µg mL^{-1} streptomycin. Culture medium was changed every 3 days. When cells were confluent, they were harvested using trypsin/EDTA (Sigma) and divided into two 25-cm^2 flasks. In this study, we used the first three passages of fibroblasts for all measurements, and in each experiment, the cells compared have all undergone the same number of passages.

Analyses of TSF proliferation ability: TSF growth rate and DNA synthesis rate

TSF proliferation ability was measured by testing the cell growth ratio and DNA synthesis rate.

Sample preparation
TSFs from six Pohn and six B6 mice (three females and three males for each type) were plated in 96-well plates (1000 cells/well) with 100 µL culture medium (as above). For each sample, cells were plated in six wells. TSF growth ratios and DNA synthesis rates were measured using an MTT cell proliferation assay kit (ATCC) and a BrdU-based cell proliferation ELISA kit (Roche), following the kit instructions.

Cell growth ratio
Ten microliter MTT reagent was added to each well and incubated with cells at 37 °C for 2.5 h. Then, 100 µL of detergent reagent was added, and samples were left at room temperature in the dark for 3.5 h. Absorbance was recorded at 570 nm (SPECTRAmax™ 250 Microplate Spectrophotometer, Molecular Devices Corp.). The absorbance on day 1 was used as a reference, and TSF growth ratios were calculated on days 2, 3, 4, 5, 6, 8, 10 and 12 using the following formula: Growth ratio (%) = $100 \times (\text{Absorbance}_{2-12 \text{ days}} - \text{Absorbance}_{\text{reference}})/\text{Absorbance}_{\text{references}}$.

DNA synthesis rate
On days 2, 3, 4, 5, 6, 8, 10 and 12, DNA synthesis rates were measured. TSFs were exposed to 10 µM BrdU for 2 h under normal culture conditions. Cells were fixed and the DNA was denatured; then the cells were incubated with anti-BrdU antibody for 1.5 h to bind the BrdU that was incorporated in the newly synthesized DNA. The immune complexes were then detected by the subsequent substrate reaction. The reaction product was quantified by measuring the absorbance at 450 nM.

Cell numbers for each sample are not identical because of the different proliferation rates. Therefore, DNA synthesis rates were standardized to the number of metabolically active cells using the following formula: DNA synthesis rate = Absorbance$_{\text{BrdU DNA synthesis}}$/Absorbance$_{\text{MTT}}$.

Apoptotic cell analyses

TSFs from three Pohn and three B6 mice were seeded in 225-cm^2 flasks (20 cells/cm^2) and cultured for 7 days. The cells were stained with phycoerythrin (PE) conjugated Annexin V and PI (Ling *et al.*, 2002) according to the manufacturer's instructions (Cat. 556422, BD PharMingen™, San Diego, CA, USA). Details are described in the online supplementary experimental procedures. This method detects both early (Annexin V +, PI –) and late (Annexin V +, PI +) apoptotic cells. Addition of early plus late gives the total number of apoptotic cells.

Morphological analysis: cell surface area

TSFs of six Pohn and six B6 mice (three females and three males for each strain) were seeded in chamber slides (20 cells/cm^2) and cultured for 9 days as described above. At days 1, 3, 6, 7, 8, and 9, TSFs were fixed with 10% (v/v) formalin and then subjected to haemotoxylin and eosin staining. Image analysis software (Metamorph) was used to calculate the flat surface area of approximately 20 cells of each sample.

Macromolecular analysis: SA-β-gal

TSFs of six Pohn and six B6 mice (three females and three males for each strain) were seeded in 24-well plates (1×10^3 cells/well). At days 3, 5, 7, 9 and 11, TSFs were tested for SA-β-gal staining. To test for H_2O_2-induced cell senescence-like changes, cells were seeded in 24-well plates (1×10^4 cells/well). After 24 h, TSFs were treated for 2 h with 10, 20, 40, 80, 160, 320, and 640 µM H_2O_2 in culture medium. Cells were then washed and incubated in fresh medium for 24 h. SA-β-gal staining method is described in the online supplementary experimental procedures.

Real-time RT-PCR expression analysis: the mRNA expression of a molecular senescence marker, cyclin-dependent kinase interacting protein (Cip1)

Sample preparation
To measure *Cip1* expression levels in normally cultivated TSFs, TSFs of Pohn and B6 mice ($n = 3-8$) were cultured in 75 cm^2 flasks (20 cells/cm^2). *Cip1* expression levels were measured on days 5 and 7. To measure the H_2O_2-induced *Cip1* expression, TSFs of three Pohn and three B6 mice were plated in 75-cm^2 flasks (1×10^6 cells/flask). After 24 h, TSFs were exposed to 160 µM H_2O_2 for 2 h. TSFs were then washed twice with PBS and cultivated in fresh culture medium. *Cip1* expression was measured 4, 8, and 24 h after H_2O_2 treatment. Untreated Pohn and B6 TSFs were used as controls.

Real-time PCR

The methods of RNA isolation and reverse transcription are described in the online supplementary experimental procedures. Primer sequences for *Cip1*, forward: 5′-ACAGGCACCATGTC-CAATCCT-3′, reverse: 5′-CGTCTCCGTGACGAAGTCAAA-3′; for internal control, β-actin, forward: 5′-ATGGAATCCTGTGGCATCCA-3′, reverse: 5′-CGCTCAGGAGGAGCAATGAT-3′. Each real-time RT-PCR analysis was performed in a total volume of 20 μL reaction mixture containing 1 μL cDNA sample (diluted 1 : 10), 10 μL 2× SYBR Green PCR Master Mix (Applied Biosystems), 5 μL RNase free water, and 2 μL gene-specific forward and reverse primer (250 nM each). Real-time RT-PCR was performed using an ABI PRISM 7500HT Sequence Detection System, with SDS version 1.2 software (Applied Biosystems). The PCR cycle conditions were as follows: 50 °C for 2 min (1 cycle), 95 °C for 10 min (1 cycle), 95 °C for 15 s, and 60 °C for 1 min (40 cycles). Every test was repeated three times.

Relative expression levels of *Cip1* in TSFs without H_2O_2 treatment are shown as fold changes (FCs) between β-*actin* and *Cip1* levels that were calculated as $2^{\wedge}(Ct_{\beta\text{-actin}} - Ct_{Cip1})$. Here, Ct refers the number of PCR amplification cycles to reach fluorescent intensity above threshold. For the FC of H_2O_2-induced *Cip1* expression, *Cip1* levels of untreated cells were used as a reference: $2^{\wedge}[(Ct_{\beta\text{-actin treated}} - Ct_{Cip1\ treated}) - (Ct_{\beta\text{-actin untreated}} - Ct_{Cip1\ untreated})]$.

Cell clone size measurement

TSFs from 15 Pohn mice (7 females, 8 males), 7 B6 mice (3 females, 4 males), 15 Pohn × B6 F_1 mice (7 females, 8 males), 162 backcrossed N2 mice (80 females and 82 males), 8 old Pohn mice (4 females, 4 males) and 6 old B6 mice (3 females, 3 males) were harvested as described and filtered through 70-μM nylon mesh (Fisher) to isolate single cells. TSFs were seeded into 25 cm^2 flasks (20 cells/cm^2) and cultured as described above. After 7 days, cells were fixed with 95% ethanol, stained with crystal violet and numbers of cells/clone were enumerated with a dissecting microscope. A cell clone was defined as a group with more than four cells. A clone size larger than 100 cells/clone was defined as a large clone, and the large clone ratio (LCR) was calculated as LCR(%) = large clone number × 100/total clone number. Cloning efficiencies ranged from 10% to 20%, and there was no significant difference in cloning efficiencies among groups compared in any experiment, not even when comparing tissues from young and old B6 and Pohn mice. There were no gender differences, so data from both genders were pooled.

QTL analyses

Genotyping

DNA of 162 N2 mice was prepared from tail samples, and genotyping was performed using single nucleotide polymorphism (SNP) markers (Myakishev *et al.*, 2001). We genotyped the entire cohort of N2 mice using SNP markers that distributed across the genome and discriminated between B6 and Pohn based on The Jackson Laboratory SNPs project (Petkov *et al.*,

2004). The initial genome-wide screen was conducted with 106 SNP markers that were spaced at about 20 cM intervals throughout the genome. After defining the chromosome regions containing the QTLs, 26 additional markers for Chr 3 and Chr X were added for higher resolution (Table S1). The estimated genetic location of the SNPs is described in the online supplementary experimental procedures.

Analyses

QTL analyses were conducted using Churchill's method (Sen & Churchill, 2001). Pseudomarker 1.02, written in MATLAB (The Mathworks Inc., Natick, MA), was used for the analyses. The software can be downloaded from http://www.jax.org/staff/churchill/labsite/index.html. This method uses multiple imputations to generate genotypes on a regular grid of genome-wide locations conditional on the observed marker data. The LOD score for each marker location was calculated by averaging the LOD scores over imputations.

Single QTL scan

A whole genome scan for each single QTL was performed at 5-cM spacing, using 64 imputations, with the full model considering gender, QTL and the interacting effect. One thousand permutations of the phenotype values were used to determine threshold values (Churchill & Doerge, 1994; Kruglyak & Lander, 1995). A value of 10% was defined as the threshold for suggestive QTLs (Kruglyak & Lander, 1995).

Pairwise scans

Whole genome pair-wise scans were performed using 5-cM spacing, with gender as an additive covariate. All possible pairs of QTL locations on each chromosome were tested for association with the LCR phenotype. The likelihoods from the full model (gender, pseudo-marker pair, and the interaction between them) and the null model (no genetic effect) were compared, and LOD scores were calculated. In addition, LOD scores from the comparisons of likelihoods from the full model and the additive model (with only the main effects of pseudo-markers and gender, but no interaction) were also calculated.

Multiple regression models

LCR value variation in the N2 population, explained by QTL and possible covariates identified from suggestive single QTL and pairwise scans, was estimated from the multiple regression models (MRMs). MRMs take into account the effects of QTL, covariate, QTL-QTL interaction, and QTL-covariate interaction. Type III sums of squares and *P*-values were calculated for all terms in the MRMs. Terms were dropped sequentially until all terms in the model were significant at the 5% level. The final model was used to estimate the portions of variations of LCR explained by each QTL, covariate, or QTL–QTL interaction.

Confidence intervals of QTL

To fine map the QTL, 2 cM spacing and 128 imputations were performed for *Fcs1* on Chr 3 and *Fcs2* on Chr X. Posterior

probability densities for QTL locations were estimated. CIs were constructed based on the density distribution of each QTL location (Sen & Churchill, 2001).

Gstm mRNA expression before and after H$_2$O$_2$ treatment

Real-time RT-PCR was performed to measure the relative mRNA expression levels of these genes. Primers are listed in Table S2. Between six and nine independent samples were compared in each group for each determination. H$_2$O$_2$ treatment, RNA extraction and real-time RT-PCR have been described previously. The following formula was used to calculate the FC in the expression of the *Gstm* family genes between Pohn and B6: TSFs: $2^{\wedge}[(Ct_{pohn\ \beta\text{-actin}} - Ct_{Pohn\ candidate}) - (Ct_{B6\ \beta\text{-actin}} - Ct_{B6\ candidate})]$.

Statistical analysis

Comparisons between groups for cell growth ratio, DNA synthesis rate, cell size, cell apoptosis, *Cip1* expression, LCR, and allele effect were performed using the unpaired Student's *t*-test. $P < 0.05$ was considered statistically significant.

Acknowledgments

References

Angello JC, Prothero J (1989) Independent evidence for a commitment model of clonal attenuation. *Mech. Ageing Dev.* **49**, 281–286.

Angello JC, Pendergrass WR, Norwood TH, Prothero J (1989) Cell enlargement: one possible mechanism underlying cellular senescence. *J. Cell. Physiol.* **140**, 288–294.

Austad SN (1996) The uses of intraspecific variation in aging research. *Exp. Gerontol.* **31**, 453–463.

Berube NG, Smith JR, Pereira-Smith OM (1998) The genetics of cellular senescence. *Am. J. Hum. Genet.* **62**, 1015–1019.

Brown JP, Wei W, Sedivy JM (1997) Bypass of senescence after disruption of p21CIP1/WAF1 gene in normal diploid human fibroblasts. *Science* **277**, 831–834.

Charlesworth B (1980) *Evolution in Age-Structured Populations*. Cambridge: Cambridge University Press.

Chen X, Zhang W, Gao YF, Su XQ, Zhai ZH (2002) Senescence-like changes induced by expression of p21 (waf1/Cip1) in NIH3T3 cell line. *Cell Res.* **12**, 229–233.

Cheng JZ, Yang Y, Singh SP, Singhal SS, Awasthi S, Pan SS, Singh SV, Zimniak P, Awasthi YC (2001) Two distinct 4-hydroxynonenal metabolizing glutathione S-transferase isozymes are differentially expressed in human tissues. *Biochem. Biophys. Res. Commun.* **282**, 1268–1274.

Churchill GA, Doerge RW (1994) Empirical threshold values for quantitative trait mapping. *Genetics* **138**, 963–971.

Cristofalo VJ, Lorenzini A, Allen RG, Torres C, Tresini M (2004) Replicative senescence: a critical review. *Mech. Ageing Dev.* **125**, 827–848.

el-Deiry WS, Tokino T, Velculescu VE, Levy DB, Parsons R, Trent JM, Lin D, Mercer WE, Kinzler KW, Vogelstein B (1993) WAF1, a potential mediator of p53 tumor suppression. *Cell* **75**, 817–825.

Geiger-Thornsberry GL, Mackay TF (2004) Quantitative trait loci affecting natural variation in *Drosophila* longevity. *Mech. Ageing Dev.* **125**, 179–189.

Gerland LM, Peyrol S, Lallemand C, Branche R, Magaud JP, Ffrench M (2003) Association of increased autophagic inclusions labeled for β-galactosidase with fibroblastic aging. *Exp. Gerontol.* **38**, 887–895.

de Haan JB, Bladier C, Lotfi-Miri M, Taylor J, Hutchinson P, Crack PJ, Hertzog P, Kola I (2004) Fibroblasts derived from *Gpx1* knockout mice display senescent-like features and are susceptible to H$_2$O$_2$-mediated cell death. *Free Radic. Biol. Med.* **36**, 53–64.

Hayflick L (1965) The limited *in vitro* lifetime of human diploid cell strains. *Exp. Cell Res.* **37**, 614–636.

Hornsby PJ (2003) Replicative senescence of human and mouse cells in culture: significance for aging research. *Mech. Ageing Dev.* **124**, 853–855.

Ishikawa T, Esterbauer H, Sies H (1986) Role of cardiac glutathione transferase and of the glutathione S-conjugate export system in biotransformation of 4-hydroxynonenal in the heart. *J. Biol. Chem.* **261**, 1576–1581.

Itahana K, Campisi J, Dimri GP (2004) Mechanisms of cellular senescence in human and mouse cells. *Biogerontology* **5**, 1–10.

Jackson AU, Galecki AT, Burke DT, Miller RA (2003) Genetic polymorphisms in mouse genes regulating age-sensitive and age-stable T cell subsets. *Genes Immun.* **4**, 30–39.

Klebanov S, Astle CM, Roderick TH, Flurkey K, Archer JR, Chen J, Harrison DE (2001a) Maximum life spans in mice are extended by wild strain alleles. *Exp. Biol. Med. (Maywood)* **226**, 854–859.

Klebanov S, Flurkey K, Roderick TH, Archer JR, Astle CM, Chen J, Harrison DE (2001b) Heritability of life span in mice and its implication for direct and indirect selection for longevity. *Genetica* **110**, 209–218.

Krishnamurthy J, Torrice C, Ramsey MR, Kovalev GI, Al-Regaiey K, Su L, Sharpless NE (2004) Ink4a/Arf expression is a biomarker of aging. *J. Clin. Invest.* **114**, 1299–1307.

Kruglyak L, Lander ES (1995) A nonparametric approach for mapping quantitative trait loci. *Genetics* **139**, 1421–1428.

Kujoth GC, Hiona A, Pugh TD, Someya S, Panzer K, Wohlgemuth SE, Hofer T, Seo AY, Sullivan R, Jobling WA et al. (2005) Mitochondrial DNA mutations, oxidative stress, and apoptosis in mammalian aging. *Science* **309**, 481–484.

Kumazaki T, Robetorye RS, Robetorye SC, Smith JR (1991) Fibronectin expression increases during in vitro cellular senescence: correlation with increased cell area. *Exp. Cell Res.* **195**, 13–19.

Ling J, Pi W, Bollag R, Zeng S, Keskintepe M, Saliman H, Krantz S, Whitney B, Tuan D (2002) The solitary long terminal repeats of ERV-9 endogenous retrovirus are conserved during primate evolution and possess enhancer activities in embryonic and hematopoietic cells. *J. Virol.* **76**, 2410–2423.

Masutomi K, Yu EY, Khurts S, Ben-Porath I, Currier JL, Metz GB, Brooks MW, Kaneko S, Murakami S, DeCaprio JA et al. (2003) Telomerase maintains telomere structure in normal human cells. *Cell* **114**, 241–253.

Mathews CE, Dunn BD, Hannigan MO, Huang CK, Leiter EH (2002) Genetic control of neutrophil superoxide production in diabetes-resistant ALR/Lt mice. *Free Radic. Biol. Med.* **32**, 744–751.

McElwee JJ, Schuster E, Blanc E, Thomas JH, Gems D (2004) Shared transcriptional signature in *Caenorhabditis elegans* Dauer larvae and

long-lived daf-2 mutants implicates detoxification system in longevity assurance. *J. Biol. Chem.* **279**, 44533–44543.

Miller RA, Chrisp C, Atchley W (2000a) Differential longevity in mouse stocks selected for early life growth trajectory. *J. Gerontol. A Biol. Sci. Med. Sci.* **55**, B455–B461.

Miller RA, Dysko R, Chrisp C, Seguin R, Linsalata L, Buehner G, HarperJM, .Austad S (2000b) Mouse stocks derived from tropical islands: new models for genetic analysis of life history traits. *J. Zool.* **250**, 95–104.

Myakishev MV, Khripin Y, Hu S, Hamer DH (2001) High-throughput SNP genotyping by allele-specific PCR with universal energy-transfer-labeled primers. *Genome Res.* **11**, 163–169.

Parrinello S, Samper E, Krtolica A, Goldstein J, Melov S, Campisi J (2003) Oxygen sensitivity severely limits the replicative lifespan of murine fibroblasts. *Nat. Cell Biol.* **5**, 741–747.

Peacocke M, Campisi J (1991) Cellular senescence: a reflection of normal growth control, differentiation, or aging? *J. Cell Biochem.* **45**, 147–155.

Pendergrass WR, Li Y, Jiang D, Wolf NS (1993) Decrease in cellular replicative potential in 'giant' mice transfected with the bovine growth hormone gene correlates to shortened life span. *J. Cell. Physiol.* **156**, 96–103.

Pendergrass WR, Li Y, Jiang D, Fei RG, Wolf NS (1995) Caloric restriction: conservation of cellular replicative capacity *in vitro* accompanies life-span extension in mice. *Exp. Cell Res.* **217**, 309–316.

Petkov PM, Ding Y, Cassell MA, Zhang W, Wagner G, Sargent EE, Asquith S, Crew V, Johnson KA, Robinson P *et al.* (2004) An efficient SNP system for mouse genome scanning and elucidating strain relationships. *Genome Res.* **14**, 1806–1811.

Pignolo RJ, Masoro EJ, Nichols WW, Bradt CI, Cristofalo VJ (1992) Skin fibroblasts from aged Fischer 344 rats undergo similar changes in replicative life span but not immortalization with caloric restriction of donors. *Exp. Cell Res.* **201**, 16–22.

Sen S, Churchill GA (2001) A statistical framework for quantitative trait mapping. *Genetics* **159**, 371–387.

Serra V, Grune T, Sitte N, Saretzki G, von Zglinicki T (2000) Telomere length as a marker of oxidative stress in primary human fibroblast cultures. *Ann. N. Y. Acad. Sci.* **908**, 327–330.

Serra V, von Zglinicki T, Lorenz M, Saretzki G (2003) Extracellular super-oxide dismutase is a major antioxidant in human fibroblasts and slows telomere shortening. *J. Biol. Chem.* **278**, 6824–6830.

Smith JR, Pereira-Smith OM, Schneider EL (1978) Colony size distributions as a measure of *in vivo* and *in vitro* aging. *Proc. Natl Acad. Sci. USA* **75**, 1353–1356.

Spitz DR, Sullivan SJ, Malcolm RR, Roberts RJ (1991) Glutathione dependent metabolism and detoxification of 4-hydroxy-2-nonenal. *Free Radic. Biol. Med.* **11**, 415–423.

Stanulis-Praeger BM (1987) Cellular senescence revisited: a review. *Mech. Ageing Dev.* **38**, 1–48.

Vaughn TT, Pletscher LS, Peripato A, King-Ellison K, Adams E, Erikson C, Cheverud JM (1999) Mapping quantitative trait loci for murine growth: a closer look at genetic architecture. *Genet. Res.* **74**, 313–322.

Williams GC (1957) Pleiotropy, natural selection, and the evolution of senescence. *Evolution* **11**, 398–411.

Wolf NS, Penn PE, Jiang D, Fei RG, Pendergrass WR (1995) Caloric restriction: conservation of in vivo cellular replicative capacity accompanies life-span extension in mice. *Exp. Cell Res.* **217**, 317–323.

Supplementary material

The following material is available from www.blackwellsynergy.com

Table S1 Estimation of SNPs' genetic location. SNPs' genetic locations were estimated as being described in Supplementary Experimental Procedures and Results.

Table S2 Gstm genes and their primers for real-time RT-PCR. Gene information was extracted from www.ensembl.org. Gene names in the table are coordinated to their location in the chromosome.

Fig. S1 A. Genome-wide QTL analysis was performed using the N2 population. Chr 1 through Chr X are represented numerically on the ordinate. The abscissa represents the LOD score. For single QTL genome-wide scanning, an experiment-wide significance (LOD > 2.37, $P < 0.1$) level of linkage is shown, determined by permutation analyses with $n = 1000$. B and C show fine mapping on Chr 3 (B) and Chr X (C). The posterior probability density (PPD, broken curved line) is a likelihood statistic that gives rise to the 95% CIs that are indicated by the horizontal gray bars.

Fig. S2 Pairwise genomes scan for the detection of gene-gene interactions affecting fibroblast LCR. The interaction LOD scores appear in the upper left triangle and the joint LOD scores appear in the lower right triangle. The vertical spectrum band to the right indicates the separate scales for the interaction and joint LOD scores (on the left and right, respectively). The red spots (circled) show the interaction of a QTL pair on Chr 4 and Chr 10.